chemistry

MDPI

Article

Influence of π-Conjugated Backbone Length and Tail Chain Number on Self-Assembly Structures of 4,6-Diamino-1,3,5-triazine Derivatives Revealed by STM

Yi Wang [1,2], Fuqiong Wang [3], Xiaoyang Zhao [1], Zhipeng Zhang [1], Yue Huang [1], Hua Zheng [2], Xiaohong Cheng [3,*] and Xinrui Miao [1,*]

[1] College of Materials Science and Engineering, South China University of Technology, Guangzhou 510640, China; 2024121@dgut.edu.cn (Y.W.)
[2] DGUT-CNAM Institute, Dongguan University of Technology, Dongguan 523007, China; zhenghua@dgut.edu.cn
[3] Key Laboratory of Medicinal Chemistry for Natural Resources, Chemistry School of Chemical Science and Technology, Yunnan University, Kunming 650091, China; wangfuqiongshida@163.com
* Correspondence: xhcheng@ynu.edu.cn (X.C.); msxrmiao@scut.edu.cn (X.M.)

Abstract

4,6-Diamino-1,3,5-triazine (DT) derivatives typically exhibit excellent liquid crystal properties, attracting numerous researchers interested in enhancing their performance. In this paper, two DT molecules (DT−10 and DT−12) are employed to elucidate the effects of their backbone length and number of branches in the tail chains on self-assembled nanostructures using scanning tunneling microscopy (STM) at the 1-octanoic acid/highly ordered pyrolytic graphite interface, compared to our previous report (2TDT−n, n = 10,12,16,18). DT−10 features a short backbone and a trialkoxy chain tail, whereas DT−12 possesses a long backbone and bifurcated chain tails. STM results reveal that DT−10 assembles into a cross-shaped nanostructure with DT head groups arranged in a head-to-head configuration stabilized by a pair of N–H···N hydrogen bindings (HBs). In contrast, DT−12 assembles into a two-row linear pattern, where DT head groups exhibit a side-by-side arrangement mediated by a pair of N–H···N HBs. Comparison with our previous findings indicates that although variations in backbone length and tail chain branching can modulate the nanostructural features of DT derivatives, the chain length of DT molecules emerges as a pivotal factor governing their assembly architecture.

Keywords: self-assembly; scanning tunneling microscopy (STM); 4,6-diamino-1,3,5-triazines; HOPG; backbone length

check for updates

Academic Editor: Matthias Lehmann

Received: 15 September 2025
Revised: 16 October 2025
Accepted: 24 October 2025
Published: 27 October 2025

Citation: Wang, Y.; Wang, F.; Zhao, X.; Zhang, Z.; Huang, Y.; Zheng, H.; Cheng, X.; Miao, X. Influence of π-Conjugated Backbone Length and Tail Chain Number on Self-Assembly Structures of 4,6-Diamino-1,3,5-triazine Derivatives Revealed by STM. *Chemistry* **2025**, *7*, 173. https://doi.org/10.3390/chemistry7060173

Copyright: © 2025 by the authors. Licensee MDPI, Basel, Switzerland. This article is an open access article distributed under the terms and conditions of the Creative Commons Attribution (CC BY) license (https://creativecommons.org/licenses/by/4.0/).

1. Introduction

Liquid crystals (LCs), typically characterized by a π-conjugated backbone and aliphatic chains, can form highly organized nanostructures [1–8]. Due to their long-range order and flowability, LCs have been extensively studied for use in applications such as liquid-crystal display (LCD) devices [9], batteries [10], biosensors, and lasers. Reasonable and rational design of molecular structure is a prerequisite for achieving macroscopic LC properties of molecules. The typical chemical structure of LC molecules comprises a π-conjugated backbone, polar groups, and aliphatic chains. As a result, molecular shape and weak intermolecular interactions play crucial roles in controlling the stability of LC phases.

Researchers in supramolecular chemistry have also shown interest in elucidating the regulatory mechanisms of LC performance, as scanning tunneling microscopy (STM)—a

technique with submolecular resolution—can provide higher-resolution and more direct visualization of self-assembled LC molecular nanostructures on surfaces [11–14]. This resolution enables observation of nanostructures formed by supramolecular self-assembly, mediated by weak interactions such as electrostatic forces, hydrogen bonding (HB) [15–17], dipole−dipole interactions [18], and van der Waals (vdW) forces [19–22]. Moreover, the principles governing the self-assembly of organic molecules on 2D surfaces may also extend to their liquid crystal states [3–5].

4,6-Diamino-1,3,5-triazine (DT) derivatives are widely investigated in diverse fields such as liquid crystals (LCs) [23], organic electronics [24], and medical applications [25], owing to their multiple efficient HB sites. Some DT derivatives with LC properties have been shown to self-assemble into two-dimensional (2D) nanostructures. For example, Meijer et al. demonstrated that π-conjugated oligo-(π-phenylenevinylene) could be utilized to fabricate columnar nanowires through the formation of a supermacrocyclic π-conjugated system [26,27]. Additionally, linear and rosette patterns were observed using STM, which depends on the ratio of side-chain length to π-conjugated backbone length [27]. However, the effects of backbone length and tail chain branching on self-assembly remain poorly understood. Therefore, the molecular self-assembly behavior of LCs, with respect to the underlying influencing factors, warrants further investigation at the molecular level.

Our previous work investigated the effect of chain length on DT derivatives (2TDT−n, n = 10, 12, 16, 18) (Figure 1a) at the 1-octanoic acid (OA)/highly ordered pyrolytic graphite (HOPG) interface [28]. The 2TDT−n molecule comprises a bulky polar DT head group, a bithiophene backbone, and a trialkoxy tail chain. We studied the effect of chain length on the self-assembled nanostructures of DT derivatives. In this extended microscopic study, two DT derivatives (DT−10 and DT−12) (Figure 1b,c) were employed to understand how backbone length and tail chain branching on the formation of self-assembled nanostructures at the OA/HOPG interface via STM. DT−10 features a short backbone and a single tail chain, whereas DT−12 possesses a long backbone and a bifurcated tail chain. These derivatives exhibit structural similarity to our previously reported 2TDT−10 and 2TDT−12 [29,30], respectively, enabling comparison of the effects of backbone length and tail chain branching on self-assembly patterns.

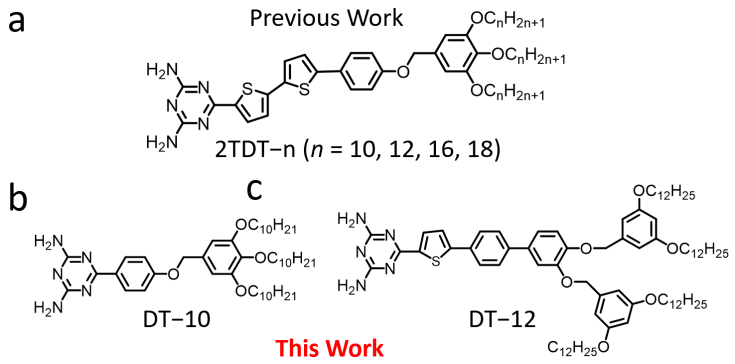


Figure 1. Chemical structures of (**a**) 2TDT−n (n = 10, 12, 16, 18) [28], (**b**) DT−10, and (**c**) DT−12 compounds.

Based on STM observations, the key factors driving the motif diversity of DT derivatives have been elucidated, providing insights for the design of surface-confined self-assembled architectures and their corresponding LC phases. Density functional theory (DFT) calculations were employed solely to optimize the backbone conformations of DT−10 and DT−12, which were used to build the models of molecular adlayers.

2. Materials and Methods

2.1. Materials

The DT−10 [31] and DT−12 molecules were synthesized and supplied by Cheng's group at Yunnan University, and the synthesis route of the DT−12 molecules is shown in Figure S1, with its ^{1}H-NRM and ^{13}C-NRM are shown in Figures S2 and S3. OA and *n*-tetradecane solvents were purchased from Aladdin Reagent Co., Ltd (Guangzhou, China). The two molecules mentioned above were used without further purification. Both molecules were dissolved in solvents at a target concentration of 10^{-4}mol/L, respectively, which act as mother liquor. Other solutions with different concentrations were acquired, diluted from mother liquor. A droplet of the sample solution was deposited onto the freshly cleaved HOPG (quality ZYB, Bruker, Billerica, MA, USA). Subsequently, STM measurements were performed on a Nanoscope IIIa Multimode SPM (Bruker, Billerica, MA, USA) at room temperature under atmospheric conditions. The tip, made of Pt/Ir material, was mechanically cut. The initial STM images were recorded in a constant current mode, then processed and analyzed using Portable Fab Viewer software (v 2.18) [32]. All molecular models were constructed with Materials Studio (v 7.0) software.

2.2. DFT Calculations

Geometry optimization of the molecular backbone was performed solely using Gaussian 09 (Rev. E.01) with the M06-2X hybrid method and the 6-31+g(d) basis set, which is a split-valence polarized basis set operating in a vacuum environment [32,33]. The optimized molecular configurations were used to construct molecular adlayer models in STM images.

3. Results and Discussion

3.1. Self-Assembling Nanostructures of DT Molecules Regulated by π-Conjugated Backbone Length

Inspired by Meijer et al. [27], and other researchers' reports [34,35], the ratio of the side chain length to the π-conjugated backbone depends on various motifs in DT derivatives. The effect of backbone length on the self-assembled nanostructures of DT has been extensively studied. Thus, a short-backbone-length molecule, DT−10 was introduced and its self-assembly behaviors were studied. After dropping a droplet of DT−10 solution in OA solvent onto a freshly cleaved HOPG substrate, the self-assembled structure formed by DT−10 was observed using STM. The large-scale STM image clearly shows that DT−10 molecules organize into a cross-shaped pattern, as depicted in Figure 2a. The π-conjugated backbones and side chains of DT−10 molecules are distinguishable in STM images due to their different electron densities. The bright rods represent the backbones of DT−10 molecules with high electron densities, while the dark stripes indicate alkoxy chains with low electron densities. In addition, there are two cavities with brighter and darker colors. More detailed information is available in the high-resolution STM image, as shown in Figure 2b and Figure S4. It reveals that the backbones of DT−10 molecules are adsorbed on the HOPG surface and form cross-shaped arrangements. Two DT−10 molecules form a dimer with a head-to-head packing arrangement, serving as the fundamental building block for this structure. Additionally, another dimer is located at the center of the first dimer and oriented perpendicularly. Four DT−10 molecules pack in a head-to-tail manner, forming a quadrangular cavity. The brightness difference between the two cavities might be derived from extensive orientation of alkoxy chains on HOPG, which can be indicated in Figure S2. Moreover, the chiral domains were also observed in Figure S5a,b based on the relative positions of the brighter and darker cavities. It is indicated that the domains shown in Figure 2a are a conglomerate of domains with different (opposite) handedness.

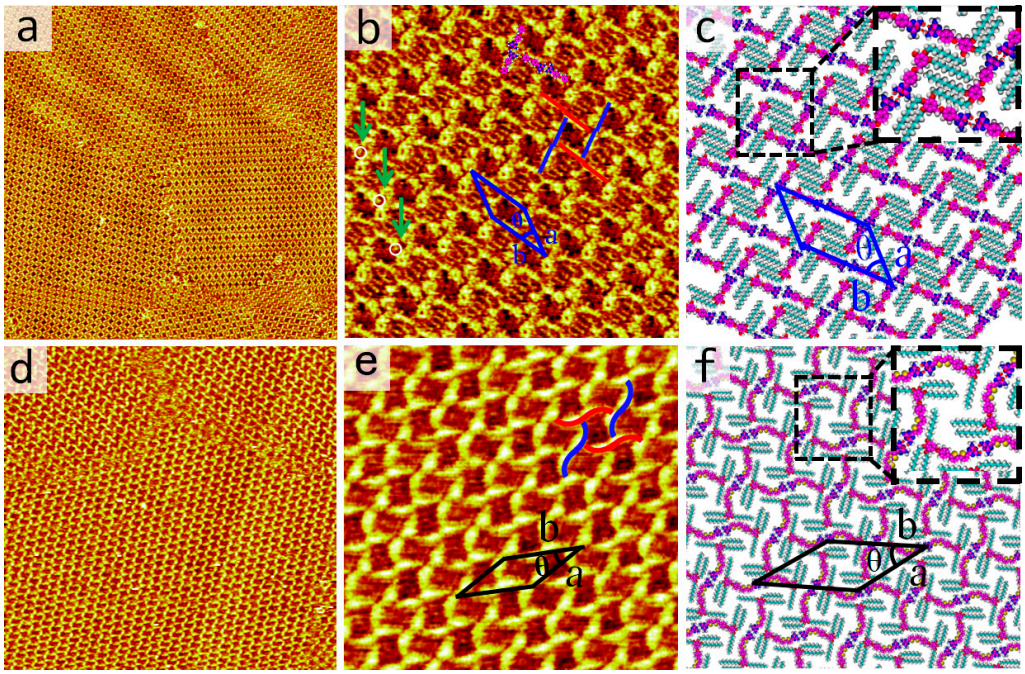


Figure 2. (**a**,**b**) Large-scale and high-resolution STM images of DT−10 at the OA/HOPG interface, respectively. Scanning Tunneling parameters: I_{set} = 400 pA, V_{bias} = 600 mV. Image sizes: (**a**) 100 × 100 nm^2, (**b**) 21 × 21 nm^2. The solid lines in red and blue represent dimers with opposite chirality, and the white circles indicate the alkyl chains which are directed to the liquid phase in (**b**). (**c**) Corresponding structural model of (**b**). The inset displays N−H···N HBs, marked by red dashed lines in the dimers. (**d**,**e**) Large-scale and high-resolution STM images of 2TDT−10 at the OA/HOPG interface, respectively. Scanning Tunneling parameters: I_{set} = 410 pA, V_{bias} = 580 mV. Image sizes: (**d**) 110 × 110 nm^2, (**e**) 25 × 25 nm^2. (**e**) The solid S-shaped lines in red and blue represent dimers of 2TDT−10 with opposite chirality. (**f**) Corresponding structural model of (**e**). The inset displays N−H···N HBs, marked by red dashed lines in the dimers.

For each DT−10 molecule, two side chains run parallel to each other and are perpendicular to the backbone. Both alkoxy side chains lie flat on the highly ordered pyrolytic graphite surface to enhance interactions with the substrate. The side chains from different molecules interdigitate to maximize van der Waals forces. Based on line profile analysis, two alkoxy side chains of a DT−10 molecule within the brighter cavities participate in interdigitation with the alkoxy chains of adjacent molecules. Concomitantly, the tails of the DT cores adopt a cross-shaped configuration perpendicular to the dimer backbone, leaving insufficient free volume to accommodate the extension of the third alkoxy chain of the DT−10 molecule. Thus, the other missing alkoxy chains in the cross-shaped pattern are believed to suspend in the solution rather than absorb on the substrate. In addition, the bright dots in the white circles in Figure 2b prove to be the sites where the alkoxy chains are perpendicular to the substrate, because the area is brighter than the other alkoxy chain areas [36].

Based on the STM data, the corresponding molecular models are constructed as shown in Figure 2c. The enlarged inset at the top right highlights N−H···N intermolecular HBs. For each dimer, a pair of N−H···N HBs, originating from the heads of DT−10 molecules, likely stabilizes the dimer. The unit cell and molecular models, overlaid on the high-resolution STM image, include four DT−10 molecules. The parameters of the unit cell are: a = 3.9 ± 0.1 nm, b = 4.8 ± 0.1 nm, and θ = 37 ± 1° (Table 1). Moreover, attempts were made with other concentrations in the OA solvent and with *n*-tetradecane as the solvent at various concentrations, but no other nanostructures were observed.

Table 1. Experimental unit cell parameters for self-assembled structures by DT−10, 2TDT−10, DT−12, and 2TDT−12, 16, and 18.

Compound	Pattern	*a* (nm)	*b* (nm)	*θ* (°)
DT−10	Cross-shaped	3.9 ± 0.1	4.8 ± 0.1	37 ± 1
2TDT−10 [28]	Four-leaved	4.5 ± 0.1	6.2 ± 0.1	40 ± 1
DT−12	Two-row linear pattern	1.7 ± 0.1	6.5 ± 0.1	75 ± 1
2TDT−12 [28]	Two-row linear pattern	1.6 ± 0.1	7.2 ± 0.1	90 ± 1
2TDT−16 [28]	Two-row linear pattern	1.2 ± 0.1	8.8 ± 0.1	90 ± 1
2TDT−18 [28]	Two-row linear pattern	1.2 ± 0.1	9.1 ± 0.3	90 ± 1

Our previous research revealed a structurally similar molecule to 2TDT−10, featuring a bulky polar DT head, a bithiophene backbone, and a tridecalkoxy wedge-shaped chain. 2TDT−10 can form an ordered four-leaved network on the HOPG surface (Figure 2d,e). Each brighter S-shaped feature contains two molecules, with the dimer serving as the self-assembled unit (Figure 2e). The S-shaped dimer adopts a head-to-head arrangement through a pair of HBs (N–H···N) in an antiparallel orientation. In contrast, the 2TDT−10 molecule has a bithiophene group on its backbone, unlike the DT−10 molecule.

Moreover, DT−10 and 2TDT−10 are both prochiral molecules. The adsorption orientation of these molecules results in the preferential alignment of one of their enantiotropic faces in contact with the highly ordered pyrolytic graphite. The molecules adsorb in a cross-shaped pattern between adjacent DT dimers. The DT side chains extend perpendicular to the direction of the dimer repeat. All molecules within a cross-shaped pattern adsorb via the two enantiotropic faces. In Figure 2b,e, while the four-fold nodes (red and blue) are racemic, the cross-shaped assembly patterns of DT−10 and 2TDT−12 molecules still exhibit chirality, as shown in Figure S5.

Comparing the current nanostructure of DT−10 with that of 2TDT−10 [28], both molecules show similar arrangements. It is reasonable to suggest that variations in the length of the π-conjugated backbone of DT derivatives do not significantly influence the assembly of these nanostructures.

3.2. How Does the Number of Branches in the Tail Chain Affect the DT Molecular Assembly?

The influence of the number of tail chains on the assembly structure of organic molecules has been reported by Kikkawa et al. [37]. While few studies have reported on the number of branches in the tail chain of DT derivatives' assembly structure, this study utilizes DT-12 molecules to investigate how the number of tail chain branches affects self-assembly motifs.

Following the same experimental steps described above, the self-assembled morphology of DT−12 molecules at the OA/HOPG interface was obtained. Figure 3a shows a large-scale STM image of the two-row linear pattern formed by DT−12. More details, including the unit cell, are displayed in the high-resolution STM image in Figure 3b. The backbones of DT−12 molecules are represented by bright bars, while the side chains appear as short, dark stripes. Two DT−12 molecules pack side-by-side in an anti-parallel arrangement to form a dimer. These dimers, serving as building blocks, are arranged in a linear pattern, resulting in a two-row linear structure. The angle between a dimer and a lamella is approximately 75°. For each DT−12 dimer, the DT groups facilitate the formation of a pair of N−H···N intermolecular HBs. By carefully counting the number of chains, it is worth noting that the two side chains of each DT−12 molecule adsorb onto the HOPG surface, while the other remains suspended in the solution due to spatial constraints. The alkoxy chains of DT−12 molecules interdigitate and align parallel to each other, maximizing van der Waals forces between the alkoxy chains and the substrate. The alkoxy chains between two neighboring stripes are fully interdigitated at an angle of (α) 89 ± 1° from the lamellae. This packing model of side chains enhances van der Waals forces between molecules and

substrate. By counting the lines, two alkoxy side chains of one DT−12 molecule within the dimer participate in interdigitation with the alkoxy chains of adjacent linear arrays, while the DT−12 cores in the dimer adopt a tightly packed configuration. This spatial arrangement leaves insufficient free space for the extension of the third and fourth alkoxy chains of the DT−12 molecule. Thus, the other missing alkoxy chains in the two-row linear pattern are believed to suspend in the solution rather than absorb on substrate. In addition, the light dots in the white circles in Figure 3b prove to be the sites where the alkoxy chains are perpendicular to the substrate, because these areas are brighter than the other alkoxy chain areas [36].

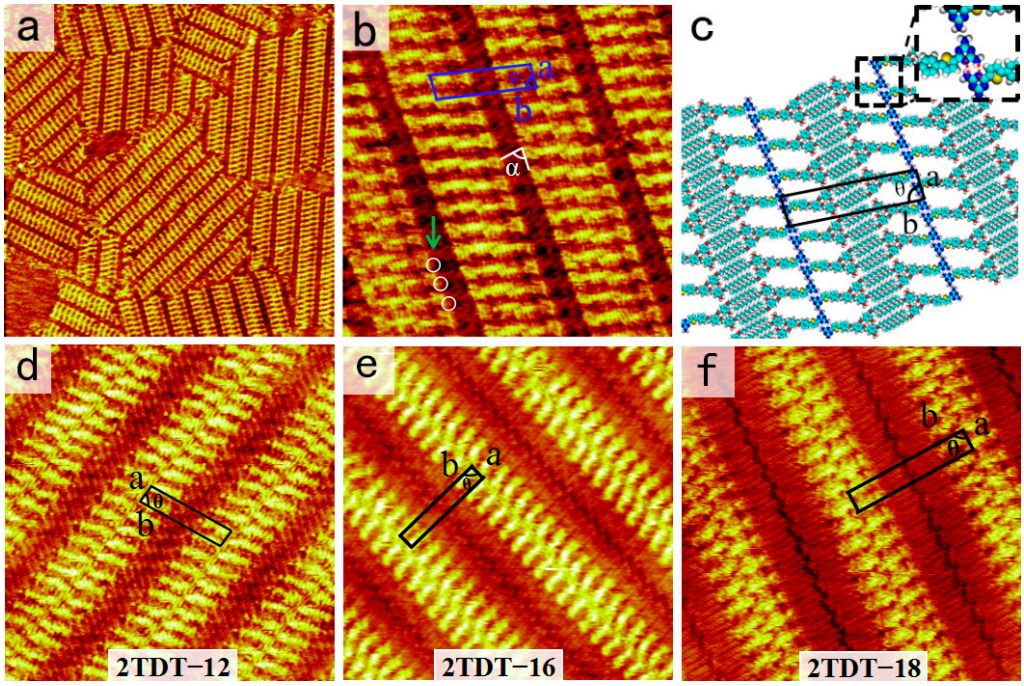


Figure 3. (**a**) Large-scale and (**b**) high-resolution STM images for the two-row linear Pattern-I nanostructure of DT−12 at the OA/HOPG interface. Tunneling parameters: I_{set} = 400 pA, V_{bias} = 600 mV. Image sizes: (**a**) 70 × 70 nm^2 and (**b**) 18 × 18 nm^2. The white circles indicate the alkyl chains which are directed to the liquid phase in (**b**). (**c**) Structural model. The inset depicts a pair of N−H···N HBs highlighted by red dashed lines in a dimer. (**d**–**f**) High-resolution STM images of the two-row linear patterns of 2TDT−12, 16, and 18 at the OA/HOPG interface. Tunneling parameters: I_{set} = 400–500 pA, V_{bias} = 600–650 mV. Image sizes: (**d**) 25 × 25 nm^2, (**e**) 18 × 18 nm^2, and (**f**) 20 × 20 nm^2.

To explain the formation mechanism of the self-assembled structure of DT−12, the proposed molecular model is shown in Figure 3c. In each dimer, the heads of two DT−12 molecules pack side by side to match their bonding sites and form a pair of N−H···N intermolecular HBs. The enlarged inset in Figure 3c depicts these HB interactions as red dashed lines. Intermolecular hydrogen bonding (HB) interactions between adjacent dimers are absent, attributed to the mismatched spatial arrangement of their respective hydrogen bonding sites. The approximate parameters of the unit cell are as follows: a = 1.7 ± 0.1 nm, b = 7.2 ± 0.1 nm, and θ = 75 ± 1°, as listed in Table 1.

Our previous work reported the self-assembled nanostructure of 2TDT−12 (Figure 3d), similar to DT−12, at the OA/HOPG interface, which shows three coexisting morphologies across the entire scan area: bamboo-like, flower-like patterns, and a two-row linear pattern [28]. However, only a two-row linear pattern is observed in the self-assembly of DT−12 and 2TDT−12 molecules. In 2TDT−12, the molecular backbone forms a two-row linear pattern, with the DT heads arranged side by side, binding via a pair of N−H···N HBs with adjacent DT heads. The angle between the lamellar axis, composed of π-conjugated groups, and

the aliphatic chains is 48 ± 1°. Additionally, there is no interdigitation of side chains in neighboring lamellae. The primary distinction between the nanostructures of DT−12 and 2TDT−12 lies in the configurational arrangement of their alkyl tail chains, with a particular emphasis on the presence or absence of interdigitation. As a result, changing the number of branches in the tail chain can slightly modify the nanostructure of the DT molecule.

To verify further whether the chain length influences molecular self-assembly as a domain factor, molecules (2TDT−16 and 2TDT−18) with longer side chains are used, and their self-assembled nanostructures at the OA/HOPG interface were also observed, respectively (Figure 3e,f). STM shows that both molecules pack into a two-row linear pattern, adopting a face-to-face arrangement. The STM results indicate that the length of the side chain is a key factor in determining the molecular packing arrangement.

4. Role of the DT Moiety

DT units with strong polarity greatly affect the adlayers of DT derivatives on the highly ordered pyrolytic graphite surface [28,29]. Meijer et al. reviewed many related studies on DT derivatives by varying the ratio between the π-conjugated backbone and the length of the aliphatic chain. They provided a detailed explanation of the typical arrangement of the DT moiety [15,27,29,38]. Our previous experiments also showed other arrangements of the DT moiety [26], though only two types of arrangements are discussed in this paper. To better distinguish the arrangement of DT units, three nitrogen atoms in each DT are labeled as positions 1 and 2 (Figure 4). Dimer I takes a typical face-to-face fashion at the 1,1 sites (Type-I), binding with a couple of N···H−N HBs, which are the main interactions creating the cross-shaped pattern in DT−10 and the four-leaf-shaped pattern in 2TDT−10. Dimer II, bonded at 2,2 sites (Type-II), mainly appears in a two-row linear pattern in DT−12 and 2TDT−12 adlayers [28].

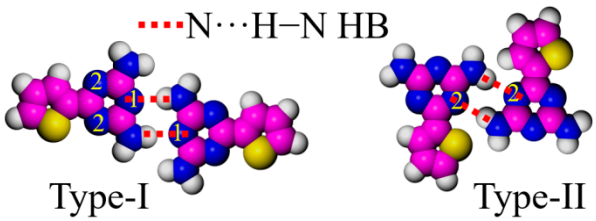


Figure 4. Arrangement models of the DT head. Carbon atoms are represented in pink, hydrogen atoms in white, nitrogen atoms in blue, sulfur atoms in yellow, respectively.

Therefore, the bonding models of DT heads in various arrangements depend on their molecular structure. This explanation is consistent with Meijer's reported chain-length effect [26]. It is well-known that the length of the side chain plays a key role in determining the binding model of DT heads [28,39].

5. Analyzing the Assembly Structures Through Unit Cell Parameters

Table 1 summarizes all patterns of DT molecules and their unit cell parameters. Due to the similar arrangement of cross-shaped (DT−10) and four-leaved (2TDT−10) patterns, the unit cell parameter b is 6.2 nm in the four-leaved pattern along the S-shaped rigid backbone, which is larger than that in the cross-shaped pattern (b = 4.8 nm) of DT−10. This difference (1.4 nm) roughly matches the discrepancy between the two π-conjugated backbone lengths (1.65 nm (4.90 nm−3.25 nm) in Figure 5), indicating that when the tridecyloxy "wedge"-shaped group acts as an end group, the π-conjugated backbone length cannot significantly tune the self-assembled pattern of DT derivatives. Additionally, comparing the parameters of the two-row linear pattern (DT−12) and two-row linear pattern (2TDT−12) reveals that the unit cell parameters a and b are nearly equal [28], and their difference stems

from the arrangement of the tail chains, specifically whether they are interdigitated or not. Therefore, variations in the tail chain branch numbers only have a slight influence on the molecular nanostructure of the DT derivatives. When the length of side chains of 2TDT−n is further increased to n = 16 and 18, the self-assembly nanostructures of 2TDT−16 and 2TDT−18 both adopt the two-row linear pattern (Figure 3e,f), the reason is that the interaction between the molecule and the substrate enhances with the length of the side chain, making it difficult for the aliphatic chain to move [28]. In addition, the unit cell parameters of b values for 2TDT−16 and 2TDT−18 are also increased to 8.8 and 9.1 from 7.2 nm in 2TDT−12, respectively. Overall, the chain length plays a crucial role in determining the arrangement of molecules rather than π-conjugated backbone length or tail chain branch numbers. That is, when the tail chain length is n = 10, the DT derivatives tend to form a cross-shape pattern, and when the tail chain length is $n \geq 12$, the molecule tends to be arranged in a two-row linear pattern.

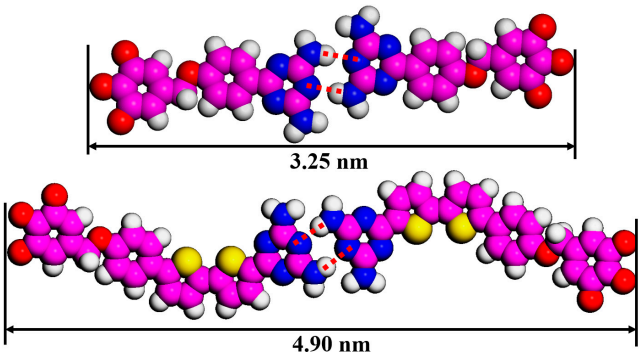


Figure 5. Measured backbone length of DT−10 and 2TDT−10 in dimers. Carbon atoms are represented in pink, hydrogen atoms in white, nitrogen atoms in blue, sulfur atoms in yellow, respectively.

6. Conclusions

In summary, two DT molecules (DT−10 and DT−12) are used to investigate how their backbone length and branch number in the tail chains influence self-assembled nanostructures, compared to our previously reported self-assembly of diverse DTs (2TDT−n, n = 10, 12, 16, 18), examined using STM at the OA/HOPG interface. The STM results show a similar arrangement between cross-shaped (DT−10) and four-leaved (2TDT−10) patterns. DT−12 and 2TDT−12 form similar structures, both adopting a two-row linear pattern. Furthermore, 2TDT−16 and 18 both adopt a two-row linear pattern. Therefore, changes in backbone length and branch number have a marginal impact on the molecular nanostructure, emphasizing that the chain length of DT molecules plays a crucial role in tuning their assembly structures. These insights help deepen understanding of self-assembly behaviors, which could be particularly important for controlling the performance of LCs.

Supplementary Materials: The following supporting information can be downloaded at: https://www.mdpi.com/article/10.3390/chemistry7060173/s1, Figure S1: A detailed procedure for the synthesis of DT−12 is given [40]; Figures S2 and S3: The ^{1}H-NMR and ^{13}C-NMR spectrums of DT−12 in CD_2H_2 solvent, respectively. Figure S4: High-resolution STM image of DT−10 at the OA/graphite interface. Figure S5: (a,b) Large-scale and high-resolution STM images of DT−10 show different chiral domains at the OA/HOPG interface, respectively.

Author Contributions: Conceptualization, Y.W. and X.Z.; methodology, F.W.; software, Y.W.; validation, F.W., Z.Z. and Y.H.; formal analysis, Z.Z.; investigation, Y.W.; resources, Z.Z.; data curation, Y.W.; writing—original draft preparation, Y.W.; writing—review and editing, X.M.; visualization, Y.W.; supervision, X.M.; project administration, H.Z.; funding acquisition, X.C. All authors have read and agreed to the published version of the manuscript.

Funding: This research was funded by the National Natural Science Foundation of China, grant number 22172055 and 22261055, and the Natural Science Foundation of Guangdong Province, grant number 2022A1515011892, the Guangdong-Taiwan Technology Cooperation Projects in Guangdong Province, grant number 2024A0505050044, and the SSL Science and Technology Commissioner Program, grant number 20234368-01KCJ-G.

Data Availability Statement: The original contributions presented in this study are included in the article material. Further inquiries can be directed to the corresponding author.

Acknowledgments: The Dongguan Key Laboratory of Digital and Intelligent Equipment for Emergency Industry and the supercomputing platform at South China University of Technology are thanked for providing the computational resources. Chunxiang Guo is acknowledged for synthesizing DT−12 during her studies at Yunnan University.

Conflicts of Interest: The authors declare no conflicts of interest.

Abbreviations

The following abbreviations are used in this manuscript:

DT	4,6-Diamino-1,3,5-triazines
OA	1-Octanoic acid
HOPG	Highly ordered pyrolytic graphite
LC	Liquid crystal
HB	Hydrogen bonding

References

1. Fuh, A.Y.G.; Cheng, K.T.; Lee, C.R. Liquid crystals biphotonic recording effect of polarization gratings based on dye-doped liquid crystal films biphotonic recording effect of polarization gratings based on dye—Doped liquid crystal films. *Liq. Cryst.* **2007**, *34*, 389–393. [CrossRef]
2. Zuo, K.; Shi, Y.; Luo, D. A review of two-dimensional liquid crystal polarization gratings. *Crystals* **2021**, *11*, 1015. [CrossRef]
3. Zhang, C.; Yu, P.; Zhao, J.; Liang, M.; He, Z.; Miao, Z. Molecular engineering controlled electric-optical performance of polymer dispersed liquid crystals. *Liq. Cryst.* **2024**, *51*, 2117–2127. [CrossRef]
4. Jeong, K.U.; Jing, A.J.; Monsdorf, B.; Graham, M.J.; Harris, F.W.; Cheng, S.Z.D. Self-assembly of chemically linked rod-disc mesogenic liquid crystals. *J. Phys. Chem. B* **2007**, *111*, 767–777. [CrossRef]
5. Jonkheijm, P.; Miura, A.; Zdanowska, M.; Hoeben, F.J.M.; De Feyter, S.; Schenning, A.P.H.J.; De Schryver, F.C.; Meijer, E.W. π-Conjugated oligo-(π-phenylenevinylene) rosettes and their tubular self-assembly. *Angew. Chem. Inter. Edit.* **2004**, *43*, 74–78. [CrossRef]
6. Pisula, W.; Tomovi, E.; Wegner, M.; Graf, R.; Pouderoijen, M.J.; Meijer, E.W.; Schenning, A.P.H.J. Liquid crystalline hydrogen bonded oligo(π-phenylenevinylene)s. *J. Mater. Chem.* **2008**, *18*, 2968–2977. [CrossRef]
7. Tschierske, C. Liquid crystal engineering-new complex mesophase structures and their relations to polymer morphologies, nanoscale patterning and crystal engineering. *Chem. Soc. Rev.* **2007**, *36*, 1930–1970. [CrossRef]
8. Ichimura, K. Photoalignment of liquid-crystal systems. *Chem. Rev.* **2000**, *100*, 1847–1874. [CrossRef]
9. Kim, T.Y.; Kim, D.S.; Ju, J.H.; Cho, W.H.; Kim, J.E.; Suh, K.S. Static charge-induced orientation of liquid crystals in LCD panels. In Proceedings of the Electrical Overstress/Electrostatic Discharge Symposium Proceedings 2010, Reno, NV, USA, 3–8 October 2010; IEEE: New York, NY, USA, 2010; pp. 1–4.
10. Su, L.; Lu, F.; Li, Y.R.; Wang, Y.Q.; Li, X.Z.; Li, Q.; Gao, X.P. Gyroid liquid crystals as quasi-solid-state electrolytes toward ultrastable zinc batteries. *ACS Nano* **2024**, *18*, 7633–7643. [CrossRef]
11. Cyr, D.M.; Venkataraman, B.; Flynn, G.W. STM investigations of organic molecules physisorbed at the liquid-solid interface. *Chem. Mater.* **1996**, *8*, 1600–1615. [CrossRef]
12. McClelland, A.A.; Ahn, S.; Matzger, A.J.; Chen, Z. Deducing 2D crystal structure at the liquid/solid interface with atomic resolution: A combined STM and SFG study. *Langmuir* **2009**, *25*, 12847–12850. [CrossRef]
13. Stabel, A.; Heinz, R.; Rabe, J.; Wegner, G.; De Schryver, F.; Corens, D.; Dehaen, W.; Süling, C. STM investigation of 2D crystals of anthrone derivatives on graphite: Analysis of molecular structure and dynamics. *J. Phys. Chem.* **1995**, *99*, 8690–8697. [CrossRef]
14. Tersoff, J.; Hamann, D.R. Theory and Application for the Scanning Tunneling Microscope. *Phys. Rev. Lett.* **1983**, *50*, 1998–2001. [CrossRef]

15. Sijbesma, R.R.; Meijer, E.B. Self-assembly of well-defined structures by hydrogen bonding. *Curr. Opin. Colloid Interface Sci.* **2010**, *30*, 24–32. [CrossRef]
16. Mohan, B.; Singh, G.; Gupta, R.K.; Sharma, P.K.; Solovev, A.A.; Pombeiro, A.J.L.; Ren, P. Hydrogen-bonded organic frameworks (HOFs): Multifunctional material on analytical monitoring. *Trac-Trend. Anal. Chem.* **2024**, *170*, 117436. [CrossRef]
17. Clair, S.; Pons, S.; Seitsonen, A.P.; BruneKlaus, H.; Barth, K.V. STM study of terephthalic acid self-assembly on Au(111): hydrogen-bonded sheets on an inhomogeneous substrate. *J. Phys. Chem. B* **2004**, *108*, 14585–14590. [CrossRef]
18. Vaughan, O.P.H.; Alavi, A.; Williams, F.J.; Lambert, R.M. Dipole amplification: A principle for the self-assembly of asymmetric monomers on metal surfaces. *Angew. Chem. Inter. Edit.* **2008**, *47*, 2422–2426. [CrossRef]
19. Liu, J.; Chen, T.; Deng, X.; Wang, D.; Pei, J.; Wan, L.J. Chiral hierarchical molecular nanostructures on two-dimensional surface by controllable trinary self-assembly. *J. Am. Chem. Soc.* **2011**, *133*, 21010–21015. [CrossRef]
20. Zhang, S.Q.; Liu, Z.Y.; Fu, W.F.; Liu, F.; Wang, C.M.; Sheng, C.Q.; Wang, Y.F.; Deng, K.; Zeng, Q.D.; Shu, L.J. Donor–acceptor conjugated macrocycles: Synthesis and host–guest coassembly with fullerene toward photovoltaic application. *ACS Nano* **2017**, *11*, 11701–11713. [CrossRef]
21. Shen, Y.T.; Guan, L.; Zhu, X.Y.; Zeng, Q.D.; Wang, C. Submolecular observation of photosensitive macrocycles and their isomerization effects on host-guest network. *J. Am. Chem. Soc.* **2009**, *131*, 6174–6180. [CrossRef]
22. Hutter, J.L.; Bechhoefer, J. Manipulation of van der Waals forces to improve image resolution in atomic-force microscopy. *J. Appl. Phys.* **1993**, *73*, 4123–4129. [CrossRef]
23. Maly, K.E.; Dauphin, C.; Wuest, J.D. Self-assembly of columnar mesophases from diaminotriazines. *J. Mater. Chem.* **2006**, *16*, 4695–4700. [CrossRef]
24. Saraswathi, S.K.; Joseph, J. Thymine-induced dynamic switching of self-assembled nanofibers in diaminotriazine-functionalized tetraphenylethylene derivatives: Implications for one-dimensional molecular devices. *ACS Appl. Nano Mater.* **2022**, *5*, 3018–3027. [CrossRef]
25. Łączkowski, K.Z.; Anusiak, J.; Świtalska, M.; Dzitko, K.; Cytarska, J.; Baranowska-Łączkowska, A.; Plech, T.; Paneth, A.; Wietrzyk, J.; Białczyk, J. Synthesis, molecular docking, ctDNA interaction, DFT calculation and evaluation of antiproliferative and anti-Toxoplasma gondii activities of 2, 4-diaminotriazine-thiazole derivatives. *Med. Chem. Res.* **2018**, *27*, 1131–1148. [CrossRef]
26. Miura, A.; Jonkheijm, P.; De Feyter, S.; Schenning, A.P.H.J.; Meijer, E.W.; De Schryver, F.C. 2D self-assembly of oligo(π-phenylene vinylene) derivatives: From dimers to chiral rosettes. *Small* **2005**, *1*, 131–137. [CrossRef] [PubMed]
27. Gesquière, A.; Jonkheijm, P.; Hoeben, F.J.M.; Schenning, A.P.H.J.; De Feyter, S.; De Schryver, F.C.; Meijer, E.W. 2D-structures of quadruple hydrogen bonded oligo(π-phenylenevinylene)s on graphite: Self-assembly behavior and expression of chirality. *Nano Lett.* **2004**, *4*, 1175–1179. [CrossRef]
28. Wang, Y.; Gao, H.; Ke, M.; Zeng, X.; Miao, X.; Cheng, X.; Deng, W. Chain-length-and concentration-dependent isomerization of bithiophenyl-based diaminotriazine derivatives in two-dimensional polymorphic self-assembly. *Langmuir* **2022**, *38*, 7005–7012. [CrossRef] [PubMed]
29. Wang, Y.; Tan, X.; Pang, P.; Li, B.; Miao, X.; Cheng, X.; Deng, W. Template-assisted 2D self-assembled chiral Kagomé network for selective adsorption of coronene. *Chem. Commun.* **2020**, *56*, 13991–13994. [CrossRef]
30. Tan, X.P.; Chang, Q.; Su, F.; Cao, Y.; Liu, F.; Cheng, X.H. Rodlike 4,6-diamino-1,3,5-triazine derivatives, effect of the core length on mesophase behavior and their application as LE-LCD device. *J. Mol. Liq.* **2022**, *346*, 117879. [CrossRef]
31. Silly, F. A robust method for processing scanning probe microscopy images and determining nanoobject position and dimensions. *J. Microsc-oxford.* **2010**, *236*, 211–218. [CrossRef]
32. Zhao, Y.; Truhlar, D.G. Density functionals with broad applicability in chemistry. *Acc. Chem. Res.* **2008**, *41*, 157–167. [CrossRef]
33. Bader, R. Atoms in molecules: A quantum theory. *J. Mol. Struct. Theochem.* **1994**, *360*, 1–3.
34. Xu, L.R.; Yang, L.; Lei, S.B. Self-assembly of conjugated oligomers and polymers at the interface: Structure and properties. *Nanoscale* **2012**, *4*, 4399–4415. [CrossRef]
35. Zhao, J.F.; Li, Y.B.; Lin, Z.Q.; Xie, L.H.; Shi, N.E.; Wu, X.K.; Wang, C.; Huang, W. Molecule length directed self-assembly behavior of tetratopic oligomeric phenylene−Ethynylenes end-capped with carboxylic groups by scanning tunneling microscopy. *J. Phys. Chem. C* **2010**, *114*, 9931–9937. [CrossRef]
36. Hu, Y.; Miao, K.; Zha, B.; Peng, S.; Xu, L.; Miao, X.Y.; Deng, W.L. STM exploration of the diverse polymorphs for tri-substituted anthraquinone derivatives via alkyl chain elongation. *Adv. Mater. Interfaces* **2016**, *3*, 1600428. [CrossRef]
37. Kikkawa, Y.; Koyama, E.; Tsuzuki, S.; Fujiwara, K.; Miyake, K.; Tokuhisa, H.; Kanesato, M. Self-assembly of bipyridine derivatives at solid/liquid interface: Effects of the number of peripheral alkyl chains and metal coordination on the two-dimensional structures. *Surf. Sci.* **2007**, *601*, 2520–2524. [CrossRef]
38. Guo, Z.; De Cat, I.; Van Averbeke, B.; Lin, J.; Wang, G.; Xu, H.; Lazzaroni, R.; Beljonne, D.; Meijer, E.W.; Schenning, A.P.H.J. Nucleoside-assisted self-assembly of oligo(π-phenylenevinylene)s at liquid/solid interface: Chirality and nanostructures. *J. Am. Chem. Soc.* **2011**, *133*, 17764–17771. [CrossRef] [PubMed]

39. Liu, C.; Gao, H.; Li, T.; Xiao, Y.; Cheng, X.H. Bisthiophene/triazole based 4,6-diamino-1,3,5-triazine triblock polyphiles: Synthesis, self-assembly and metal binding properties. *J. Mol. Struct.* **2019**, *1193*, 294–302. [CrossRef]
40. Hu, Y.; Miao, K.; Zha, B.; Miao, X.R.; Xu, L.; Deng, W.L. Side chain position, length and odd/even effects on the 2D self-assembly of mono-substituted anthraquinone derivatives at the liquid/solid interface. *RSC Adv.* **2015**, *5*, 93337–93346. [CrossRef]

Disclaimer/Publisher's Note: The statements, opinions and data contained in all publications are solely those of the individual author(s) and contributor(s) and not of MDPI and/or the editor(s). MDPI and/or the editor(s) disclaim responsibility for any injury to people or property resulting from any ideas, methods, instructions or products referred to in the content.